Research Article | Vol. 29, No. 26 / 20 Dec 2021 / Optics Express 42978
Optics EXPRESS

Refractive index sensing by asymmetric dielectric gratings with both bound states in the continuum and guided mode resonances

CHUANBAO LIU,[1,2] YANG BAI,[3,4,*] JI ZHOU,[2] JUNHONG CHEN,[1] AND LIJIE QIAO[3,4]

[1] School of Materials Science and Engineering, University of Science and Technology Beijing, Beijing 100083, China
[2] State Key Laboratory of New Ceramics and Fine Processing, Tsinghua University, Beijing 100084, China
[3] Beijing Advanced Innovation Center for Materials Genome Engineering, University of Science and Technology Beijing, Beijing 100083, China
[4] Institute for Advanced Materials and Technology, University of Science and Technology Beijing, Beijing 100083, China
[*] baiy@mater.ustb.edu.cn

Abstract: Guided mode resonances (GMRs) and bounded states in the continuum (BICs), both supported by dielectric gratings, can realize ultrahigh Q-factors and strong localized field enhancements, beneficial to high-performance sensing applications. In this paper, based on GMR theory and numerical simulations, we systematically investigate the relationship between different order GMRs and BICs/quasi-BICs in Si-based dielectric gratings with symmetric, singly, and doubly asymmetric profiles. The introduction of broken-symmetry in adjacent gaps or Si nanobeams brings about new GRM and symmetry-protected BIC and can transform the fundamental BIC into a resonant state with finite Q-factor as high diffraction orders. A Friedric-Wintgen BIC is also achieved under normal incidence by breaking symmetries of both gaps and Si nanobeams. Further, the asymmetric dielectric gratings with high Q-factor quasi-BICs are designed as a refractive index sensor. Although the Q-factor and localized electric field penetrating into the vacuum are greatly improved with the decreasing asymmetry parameter, the sensitivity is almost unchanged while the FOM demonstrates an inverse square dependence on the asymmetry parameter. To further improve the sensitivity, we construct an asymmetric dielectric grating with a low fill factor and a big period, which manifests an excellent sensing performance with a near theoretical sensitivity limit of ~1506 nm/RIU and an ultrahigh FOM of ~5000.

© 2021 Optica Publishing Group under the terms of the Optica Open Access Publishing Agreement

1. Introduction

In the field of optical manipulation, electromagnetic resonances play an important role in the far-field and near-field wave phenomena [1–8]. Especially for resonances with high Q-factors, they are usually accompanied by the strong near-field enhancement, facilitating to light-matter interactions and promising applications in nonlinear optics [9–12], biochemical sensors [13,14], and etc. To date, various types of resonances have been proposed to achieve high Q-factors or narrow linewidths, such as plasmonic resonances in metallic structures [15], Mie resonances in dielectric structures [16], and other resonances in different geometries of structures [17]. Among them, dielectric gratings or photonic crystal slabs which support in-plane guide mode resonances (GMRs) have been extensively studied from early on and continue to the present day due to their versatile natures and easy implementation [18–21]. By controlling the period, fill factor, thickness, permittivity, and incident angle, dielectric gratings with GMRs are capable of controlling the far-field spectra and near-field distribution for a wide range of applications [20]. The GMRs,

#446937 https://doi.org/10.1364/OE.446937
Journal © 2021 Received 27 Oct 2021; revised 29 Nov 2021; accepted 29 Nov 2021; published 8 Dec 2021

Optics EXPRESS

also referred to as leaky waves, which reside above the light line and can couple to the incident propagating wave. The interference between GMRs and non-resonant transmission/reflection background provided by the effective dielectric slab will result in asymmetric Fano line shapes [19]. To achieve high Q-factors of GMRs or Fano resonances, a routine way is to decrease the amplitude modulation in dielectric gratings [18]. However, the existence of radiation channel keeps the Q-factor from diverging, i.e., the mode cannot be ideally confined. In addition, the implement of extreme conditions for small amplitude modulation, e.g., decreasing the gap size, is limited by the nanofabrication resolution. Introducing point or line defects in dielectric gratings can indeed enhance the Fano resonance and elevate the Q-factor [22–24], but the isolated defects make the features of Fano resonance inhomogeneous localized and easily disturbed by the beam diameter and the illumination position [25].

Recent studies show dielectric gratings also support non-radiating resonant states (bound states in the continuum, BICs) which have infinite radiative Q-factors within the radiation continuum but completely decouple from the outgoing waves [26–31]. According to the formation mechanism, BICs mainly manifest themselves as symmetry-protected and Friedric-Wintgen scenarios [28]. The former is derived from the symmetry incompatibility between mode's field distribution and outgoing waves; while the latter results from the destructive interference of different resonance modes. A true BIC is a mathematic concept with infinite Q-factor that only exists in the lossless and infinite structures, and cannot be detected by far-field spectra due to the non-existence of radiative channels. For real systems, any external perturbations, such as surface roughness, material loss, and finite size, can make the BIC collapse into a quasi-BIC with finite Q-factor and detectable [32–34]. Physically, BICs and GMRs in symmetric dielectric gratings are both above the light line and can be interpreted as the coupling of two in-plane counterpropagating leaky modes out of phase and in phase under normal incidence, resulting in the quenched radiation and enhanced radiation, respectively. At oblique incidence, the symmetry-protected BICs are broken and transformed into quasi-BICs with finite Q-factors, i.e., GMRs. Therefore, a splitting phenomenon of GMRs is reflected in the spectra when the incident angle is changed from normal to oblique. Although some of references have involved the BICs/quasi-BICs and GMRs, their intrinsic relevance including fundamental and high orders is not fully clarified and often refer to the highly symmetric gratings. Dielectric gratings with asymmetry profiles or complex lattices which have more degrees of freedom to customize functionalities, such as narrow linewidth bandpass filters, polarizer, and wideband anti-reflector, are rarely discussed [35]. On the other hand, by controlling the asymmetry parameters for symmetry-protected BICs or by continuously varying structure parameters for Friedric-Wintgen BICs, one can get ultrahigh Q-factors contributing to the greatly enhanced electromagnetic field into the sensing area and strong light-mater interactions, and using for the refractive index sensors and nonlinear optics [36–39]. In terms of the refractive index sensor, the relationship between asymmetry parameter and Q-factor of quasi-BICs presenting an inverse square dependence has been extensively studied and clearly elucidated [40,41], but their contributions to sensitivity (S) and figure of merit (FOM) are not well explored which are two important indicators to measure sensing performance.

In this paper, based on GMR theory and numerical simulations, we reveal the relationship between GMRs and BICs/quasi-BICs in dielectric gratings with symmetric and asymmetric profiles by controlling the width of two adjacent gaps or/and Si dielectric nanobeams. And then, the asymmetric dielectric grating with high Q-factors is served as a refractive index sensor to explore the effect of asymmetry parameters of structure on the sensing capabilities. Finally, we achieve a high-performance refractive index sensor with a sensitivity of near theoretical limit and an ultrahigh figure of merit.

Optics EXPRESS

2. Results and discussion

2.1. Singly asymmetric dielectric gratings

The geometry of our studied structures is sketched in Fig. 1, where one-dimensional infinite dielectric gratings consisting of Si nanobeams ($n_d = 3.5$) are suspended in the vacuum ($n_s = 1.0$) and normally incident by a TM-polarized plane wave ($H//y$). The thickness of dielectric gratings is $h = 230$ nm. The sum of two adjacent Si nanobeams widths and gaps are $w_1 + w_2 = 1000$ nm and $g_1 + g_2 = 320$ nm, respectively. To symmetrically study the resonance properties in dielectric gratings with symmetric and asymmetric profiles, we will regulate the adjacent Si nanobeams widths (gaps) in the following study, and adopt a dimensionless parameter defined as $\alpha_w = |w_1 - w_2|/(w_1 + w_2)$ ($\alpha_g = |g_1 - g_2|/(g_1 + g_2)$) to measure the asymmetry degree of Si nanobeams widths (gaps). Besides, independent calculations of spectral and eigenmode analysis are carried out with Comsol Multiphysics software.

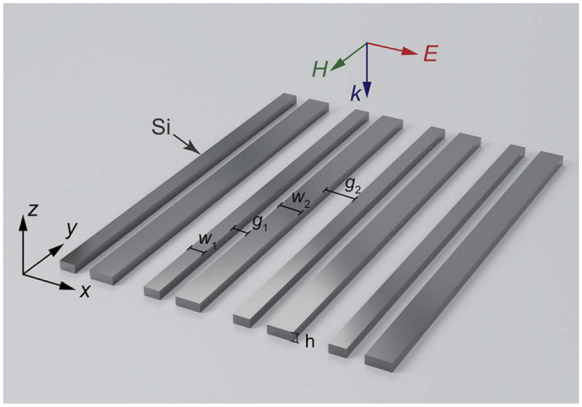

Fig. 1. Schematic of infinite planar array consisting of Si dielectric gratings under TM-polarized plane wave.

We first start with the highly symmetric dielectric gratings of $w_1 = w_2 = 500$ nm and $g_1 = g_2 = 160$ nm ($\alpha_w = \alpha_g = 0$). Under normal incidence, the reflectance spectrum manifests a weak Fano resonance with asymmetry line shape around 275 THz seemingly, after the constructive Fabry-Perot (F-P) interference (~193 THz), as illustrated in the lower panel in Fig. 2(a). This Fano resonance arises from the coupling between in-plane discrete GMR and vertical continuum F-P interference. The reflectance maximum and minimum are derived from the constructive and destructive interference between discrete and continuum states, respectively [20]. In theory, the resonant frequency of GMR can be calculated by solving the characteristic equation of homogeneous and uniaxial slab dielectric waveguide for TM mode [42,43]

$$\kappa h = m\pi + 2\text{atan}(\tilde{\varepsilon} q/\kappa), \tag{1}$$

where

$$\kappa = \sqrt{k_0^2 \bar{\varepsilon} - (\bar{\varepsilon}/\tilde{\varepsilon})\beta^2}, \quad q = \sqrt{\beta^2 - n_s^2 k_0^2} \tag{2}$$

are the wave vector components along the z-axis direction in the equivalent dielectric slab and vacuum, respectively. $\bar{\varepsilon} = (1 - F)n_s^2 + Fn_d^2$ and $\tilde{\varepsilon} = (\frac{1-F}{n_s^2} + \frac{F}{n_d^2})^{-1}$ are the zeroth-order approximation of effective permittivity for TE and TM polarizations, respectively. F is the fill factor of Si nanobeams, and k_0 is the wave number in the vacuum. $m = 0, 1, 2\ldots$ is an integer that denotes the number of magnetic modes with zero-field along z-axis direction. $\beta = 2n\pi/p_x$ is the propagation constant of n-order GMR, where $n = 1, 2, 3\ldots$ is the number of complete cycles

Optics EXPRESS

in per unit cell, p_x is the periodicity of dielectric gratings. By inserting Eq. (2) into (1), we can calculate the theoretical frequencies of different order guided mode resonances (GMR_{mn}).

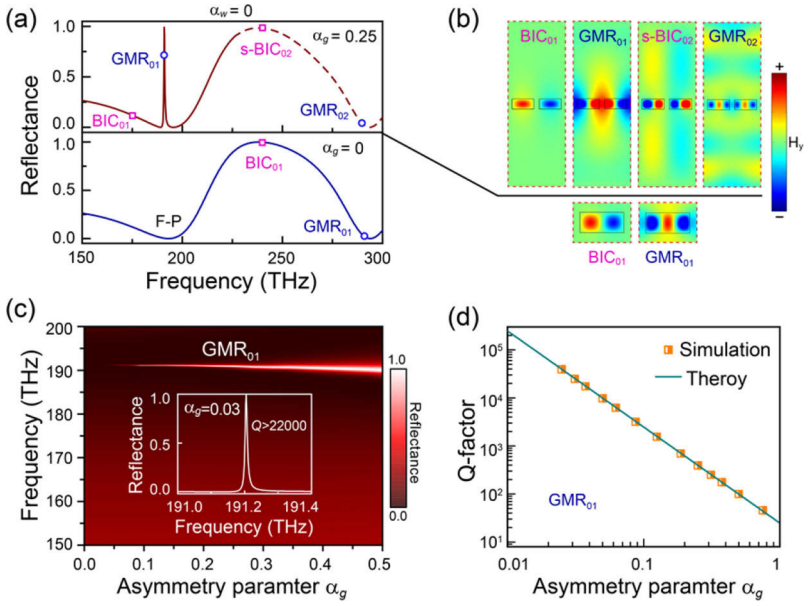

Fig. 2. Scattering properties of the symmetric and singly gap-asymmetric dielectric gratings. (a) Reflectance spectra for the gap-asymmetric (upper panel, $\alpha_g = 0.25$) and symmetric (lower panel, $\alpha_g = 0$) dielectric gratings. Blue circles and magenta squares indicate the eigenmodes of GMRs and BICs, respectively. (b) Magnetic-field profile H_y of the BICs and GMRs in (a). (c) Reflectance spectra with respect to asymmetry parameter α_g and frequency. The inset shows the reflectance spectra for $\alpha_g = 0.03$. (d) Dependence of the Q-factor on the asymmetry parameter α_g for GMR_{01}, based on simulations (orange marks) and theory prediction (cyan line).

According to the magnetic field distribution (lower-right panel, Fig. 2(b)) performed by the eigenmode analysis, this Fano resonance corresponds to the fundamental GMR_{01}. Therefore, based on Eqs. (1) and (2), we calculate the theoretical resonant frequency of GMR_{01} which is about 304.0 THz and consistent with the simulated complex eigenfrequency of 292.8 + 19.4i THz. A little deviation is mainly attributed to the inaccurate description of effective permittivity for the big periodicity-to-wavelength structures [44]. Apart from the fundamental GMR_{01}, symmetric dielectric gratings under normal incidence also support the symmetry-protected BICs with infinite radiative Q-factors. The eigenmode analysis reveals that an anti-symmetric magnetic field distribution with respect to the mirror-symmetry plane of the structure (lower-left panel, Fig. 1(b)) appears at 240.2 THz, leading to the symmetry incompatibility with outgoing fields and the formation of an ideal bound state-BIC_{01}. The subscript of BIC_{mn} also refers to the definition of m and n in the GMR theory.

Subsequently, we investigate the resonance characteristics of singly gap-asymmetric dielectric gratings by breaking the symmetry of adjacent gaps while keeping Si nanobeams unchanged. As illustrated in the upper panel of Fig. 2(a), the simulated reflectance spectrum for $\alpha_g = 0.25$ ($\alpha_w = 0$) demonstrates a similar profile to the symmetric structure ($\alpha_g = \alpha_w = 0$), but a new and sharp Fano resonance emerges at low frequency 191.0 THz. It is noted that when the incident frequency is above 227.3 THz, the reflectance spectrum is allowed high-order propagating diffractions, but still dominated by the zero-order diffraction which is displayed with the dashed line. To explore resonance features in the gap-asymmetric dielectric gratings, we perform the

Optics EXPRESS

eigenmode analysis and plot the magnetic field distributions (upper panel, Fig. 2(b)). Due to the double periodicity and unchanged fill factor F (effective permittivity), the GMR_{02} and s-BIC_{02} have approximate resonant frequencies and similar magnetic field distributions with GMR_{01} and BIC_{01} in symmetric dielectric gratings (Fig. 2(b)). However, for the s-BIC_{02}, the existence of high order propagating diffractions transforms bound state into a leaky mode with finite radiative Q-factor ($240.2 + 0.07i$ THz), and forms the characteristic interference pattern, as shown in the upper-third panel of Fig. 2(b). Since the reflectance spectrum doesn't show a sharp variation of resonance signal, this implicit leaky mode is marked as a spoof BIC_{02} (s-BIC_{02}). In addition, the eigenmode analysis shows that the newly introduced Fano resonance at 191.0 THz is attributed to the fundamental GMR_{01} (upper-second panel, Fig. 2(b)), which coincides with the theoretical calculation of 200.0 THz well, based on Eqs. (1) and (2). For the gap-asymmetric dielectric gratings under normal incidence, they still possess a mirror-symmetry plane in each unit cell and support a symmetry-protected BIC_{01} at 175.0 THz with anti-symmetric magnetic field distribution (upper-first panel, Fig. 2(b)).

Aiming at the GMR_{01} in singly gap-asymmetric dielectric gratings, spectra analysis under normal incidence is executed via continuous tuning of α_g, as shown in Fig. 2(c). We observe that the linewidth of GMR_{01} resonance decreases with decreasing the asymmetry parameter α_g and vanishes when the singly gap-asymmetric dielectric gratings return to the symmetric dielectric gratings. By using the returned complex eigenfrequencies ($Q = \mathrm{Re}(f)/2\mathrm{Im}(f)$), we calculate the radiative Q-factor of GMR_{01} (squares) which demonstrates an inverse square dependence on asymmetry parameter α_g and agrees with the theory prediction well ($Q = 24.8\alpha_g^{-2}$, solid line), as shown in Fig. 2(d) [40]. It should be emphasized that this fundamental GMR_{01} cannot be transformed into a bound state due to its non-eigenfrequency in the symmetric dielectric gratings. Nevertheless, it doesn't affect the acquisition of arbitrary Q-factor resonances by controlling the difference between adjacent gaps, i.e., asymmetry parameter α_g. For example, when $\alpha_g = 0.03$, the Q-factor exceeds 22000 around 191.2 THz (inset of Fig. 2(c)). Apart from the controllable resonance linewidths or Q-factors, the coupling between GMR_{01} and constructive F-P interference makes the reflectance spectrum present two nulls on both sides of the peak, facilitating to a high-performance reflection filter.

Similarly, we break the symmetry of two adjacent Si nanobeams widths but keep the same gaps to achieve the singly Si-asymmetric dielectric gratings. The lower panel of Fig. 3(a) depicts the reflectance spectrum for $\alpha_w = 0.1$ ($\alpha_g = 0$) where a sharp GMR'_{01} and a tacit BIC_{01} with symmetric and anti-symmetric magnetic field distribution appear at 175.0 THz and 190.9 THz, respectively. Compared with the GMR_{01} in gap-asymmetric dielectric gratings (upper panel, Fig. 2(a)), the GMR'_{01} in Si-asymmetric dielectric gratings has a lower resonant frequency, resulting from the non-uniform distribution of localized field (mainly confined in nanobeams, lower panel of Fig. 3(a)) and corresponding a larger effective permittivity of dielectric gratings.

2.2. Doubly asymmetric dielectric gratings

Furthermore, the symmetry of Si nanobeams and gaps are broken simultaneously to construct doubly asymmetric dielectric gratings. Under normal incidence, the simulated reflectance spectrum for $\alpha_g = 0.25$ and $\alpha_w = 0.1$ (upper panel, Fig. 3(a)) exhibits two sharp resonances around 175.1 and 190.6 THz which can be regarded as two quasi-BICs with finite radiative Q-factors and transformed into ideal BICs when the doubly asymmetric dielectric gratings return to singly asymmetric dielectric gratings (upper panel of Fig. 2(a) and lower panel of Fig. 3(a)). Outwardly, these two quasi-BICs are determined by the Si and gap asymmetry, respectively. But essentially, they are ascribed to the formation of two fundamental guided mode resonances (GMR'_{01} and GMR_{01}), just with different localized field distributions. As shown in the insets of upper panel of Fig. 3(a), magnetic field distributions present quasi-symmetric and quasi-anti-symmetric features for GMR'_{01} and GMR_{01}, respectively. By independently

Optics EXPRESS

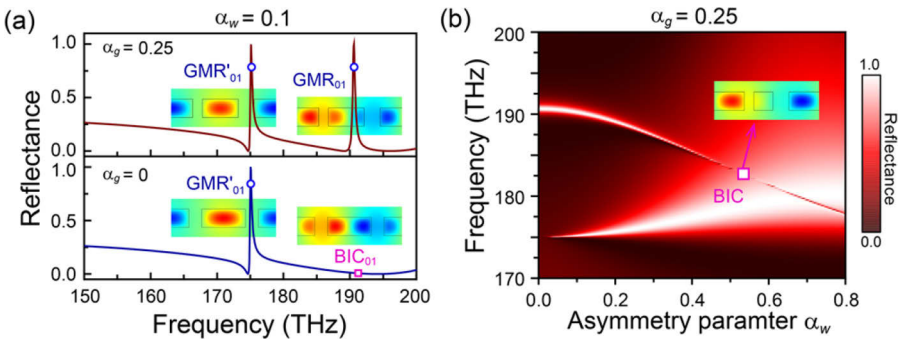

Fig. 3. Scattering properties of the singly Si-asymmetric and doubly asymmetric dielectric gratings. (a) Reflectance spectra for doubly asymmetric (upper panel, $\alpha_w = 0.1$ & $\alpha_g = 0.25$) and singly Si-asymmetric (lower panel, $\alpha_w = 0.1$ & $\alpha_g = 0$) dielectric gratings. The insets show the magnetic field profile H_y of the BICs and GMRs. (b) Reflectance spectra with respect to asymmetry parameter α_w and frequency. Magenta square indicates the position of Friedrich-Wintgen BIC. The insert shows the magnetic field profile H_y of BIC.

controlling the asymmetry parameters of α_g and α_w, we can realize versatile functionalities, such as broadband reflector, antireflection element, and bandpass filter, based on the coupling of two fundamental GMRs in doubly asymmetric dielectric gratings [35].

Figure 3(b) shows the reflectance spectra of doubly asymmetric dielectric gratings for varying frequencies and asymmetry parameter α_w ($\alpha_g = 0.25$). The linewidth of GMR$'_{01}$ increases with α_w and agrees with the theory predication for symmetry-protected quasi-BICs ($f_{FWHM} \propto \alpha_w^2$, not shown). However, the change of α_w also has an impact on the linewidth of GMR$_{01}$ despite of the unchanged α_g. As shown in Fig. 3(b), the linewidth of GMR$'_{01}$ first decreases and then increases with the increase of α_w. Especially at $\alpha_w = 0.52$, the resonant linewidth (Q-factor) tends to vanish (infinity), i.e., an ideal bound state. This type of bound state is referred to the Friedric-Wintgen BIC, owing to the destructive interference of GMR$_{01}$ and GMR$'_{01}$. According to the eigenmode analysis (insert of Fig. 3(c)), the magnetic field distribution demonstrates an anti-symmetric feature with respect to the mid-plane of unit cell, despite the structure of doubly asymmetric dielectric gratings is without any inversion symmetry. Thus, the resonant state with zero effective magnetic dipole moment is completely confined as a bound state and decoupled from the outgoing waves.

2.3. Refractive index sensor

As mentioned above, we can obtain extremely high Q-factor resonances by decreasing the asymmetry parameter α_g or α_w, which are strongly desired for sensing applications, such as refractive index, humidity, and biochemical sensors. In this section, we will investigate the sensing property of GMRs in asymmetric dielectric gratings by varying the asymmetry parameter and refractive index of surrounding medium. Figure 4(a) shows the simulated reflectance spectra when the doubly asymmetric dielectric gratings ($\alpha_g = 0.25$ and $\alpha_w = 0.1$) are immersed in different refractive index of gaseous medium from 1.00 to 1.04. The sharp reflectance peaks show a remarkable red shift for both GMR$'_{01}$ and GMR$_{01}$, even though a small fluctuation ($\Delta n_s = 0.01$). To characterize the sensing performance, two important quantities of sensitivity (S) and figure of merit (FOM), respectively, defined as resonant wavelength shift per the refractive index change unit ($S = \Delta\lambda_{res}/\Delta n_s$) and sensitivity over the full width at half maximum ($FOM = S/\lambda_{FWMH}$) are employed. By extracting reflection peak positions from Fig. 4(a) and plotting them as a function of ambient refractive index, the fitted curve presents a good linearity (Fig. 4(b)). For the GMR$'_{01}$ and GMR$_{01}$, the slopes or sensitivities are 680 and 1143 nm/RIU, respectively. If taking the

Optics EXPRESS

resonance bandwidths (λ_{FWMH} ~ 3.7 and ~3.6 nm) into account, the FOM of refractive index sensor for GMR′$_{01}$ and GMR$_{01}$ correspond respectively to 183.8 and 317.5. It is observed that although the Q-factor of GMR$_{01}$ (~441) is slightly lower than GMR′$_{01}$ (~463), the localized field is prominently penetrated into the vacuum (upper panel, Fig. 3(a)), leading to a higher sensitivity to the change in refractive index of surrounding medium and a high FOM.

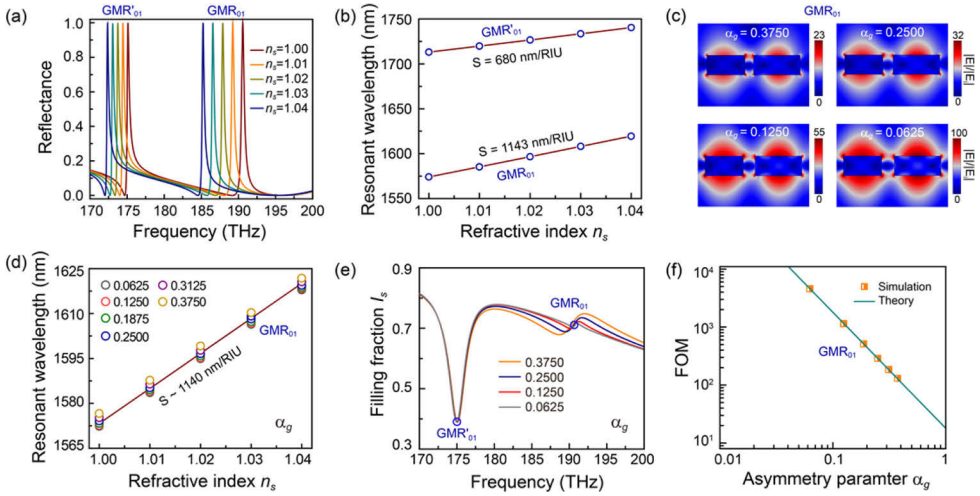

Fig. 4. Doubly asymmetric dielectric gratings with $\alpha_w = 0.1$ as a refractive index sensor. (a) The reflectance spectra of the doubly asymmetric dielectric gratings ($\alpha_g = 0.25$) for gaseous medium with different refractive indices. (b) The blue circles are the reflectance peak positions extracted from (a) and plotted against n_s. The wine line is a linear fitting curve. (c) Normalized electric field distribution for GMR$_{01}$ with different α_g. (d) The simulated reflectance peak positions for GMR$_{01}$ with different α_g and fitted curve. (e) Calculated filling fraction I_s for different α_g. (f) Dependence of FOM on α_g for GMR$_{01}$, based on simulations (orange marks) and perturbation theory (cyan line).

To give deep insight into the nature of sensitivity, an analytic formula can be deduced by the first-order electromagnetic perturbation theory [41,45]

$$S = \lambda_{res} I_s / n_s \tag{3}$$

where λ_{res} and n_s are the resonant wavelength and refractive index of surrounding medium, respectively. $I_s = \int_{S_{vac}} n_s^2 |E|^2 dxdz / \int_{S_{vac+Si}} n^2(x,y)|E|^2 dxdz$ is the filling fraction or optical overlap integral which describes the electric field energy ratio of vacuum-part to elementary cell. The Eq. (3), indicating a constant sensitivity, is only valid for single mode with a smallness of Δn_s. If the refractive index of surrounding medium has a wide variation range, non-linear or exponential behavior happen due to the non-negligible modification from the effective permittivity of dielectric gratings [46]. According to the simulated electric field distribution, we calculate the filling fractions I_s of 0.39 and 0.71 for GMR′$_{01}$ and GMR$_{01}$ of doubly asymmetric dielectric gratings ($\alpha_g = 0.25$ and $\alpha_w = 0.1$), respectively (Fig. 4(e)). The theoretical sensitivities of GMR′$_{01}$ and GMR$_{01}$ based on Eq. (3) are 668 and 1118 nm/RIU, and in accordance with the simulated results well (Fig. 4(b)).

Since the superior sensing performance, we mainly focus on GMR$_{01}$ caused by the asymmetry of gaps and explore the effect of asymmetry parameter α_g on the sensitivity and FOM. As expected, the decrease of asymmetry parameter α_g will shrink the resonant linewidth of GMR$_{01}$ and enhance the localized field around dielectric gratings. As illustrated in Fig. 4(c), the maximum enhancement factor of electric field ($|E|/|E_i|$) grows from 23 to 100 when the α_g is decreased

Optics EXPRESS

from 0.3750 to 0.0625. Intuitively, a bigger localized field in the vacuum is favorable to the light-matter interaction, and results in a higher sensitivity to the external perturbation. However, further simulations suggest that the sensitivity of refractive index sensor tends to invariability with S ~ 1140 nm/RIU, owing to the hardly shifted resonant wavelengths and filling fractions I_s for different α_g (Figs. 4(d) and 4(e)). With the decrease of α_g, the localized electric field in the vacuum and Si nanobeams both increase with same multiples, leading to an unchanged filling fraction I_s and effective permittivity referring to the Maxwell-Garnett theory [47], i.e., a constant resonant wavelength. Note that although the sensitivity tends to invariability, the FOM of refractive index sensor presents an inverse square dependence on asymmetry parameter α_g due to the shrinking resonant linewidth (FOM $\propto\alpha_g^{-2}$, Fig. 4(f)).

An effective approach is to reduce the effective permittivity of dielectric gratings which enables more electric field energy to localize in vacuum and thus increases the filling fraction I_s. But it also brings about a blue shift to the resonant wavelength at the same time, going against the improvement of sensitivity. Therefore, we extend the period to overcome above contradiction. Based on the Eqs. (1) and (2), we first theoretically calculate the sensing performance of isotropic slab dielectric waveguide with a thickness of 230 nm, as shown in Fig. 5(a). The collocation of dielectric constant ε and period p is set deliberately to excite the fundamental GMR_{01} at the same wavelength. It is observed that the sensitivity is increased with the decrease of n_s, verifying the above solution. Furthermore, we construct a singly gap-asymmetric dielectric grating with a large period of 1480 nm and a low fill factor of 0.27, which demonstrates a similar resonant wavelength of GMR_{01} in Fig. 4(a) but an obviously improved filling fraction I_s (lower panel of Fig. 5(b)). The simulated reflectance spectra shows that the resonant peak position of GMR_{01} is shifted from 1570.2 nm to 1630.4 nm when the n_s is varied from 1.00 to 1.04, as shown in the upper panel of Fig. 5(b). The slope of linear fitting is about 1506 nm/RIU (Fig. 5(c)) which approximates the theoretical sensitivity limit of $S_{max} = \lambda_{res}/n_s \approx$ 1570 nm/RIU ($I_s = 1.0$). In addition, due to a detection-limited linewidth of ~ 0.3 nm (upper panel of Fig. 5(b)), the FOM reaches ~5000 and can be further improved by decreasing the asymmetry parameter α_g.

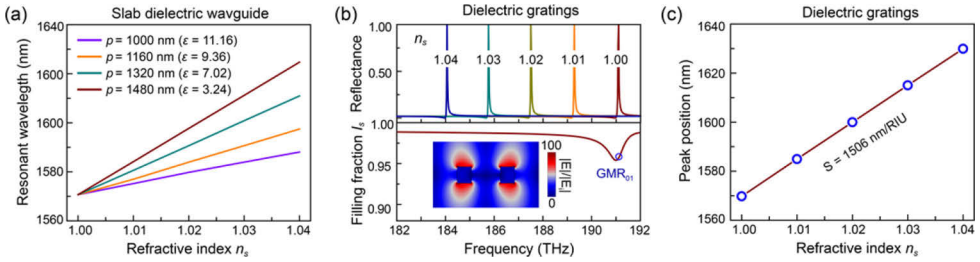

Fig. 5. A strategy to improve the sensitivity of refractive index sensor. (a) The theoretically calculated resonant wavelengths of isotropic slab dielectric waveguide with different periodicities and dielectric constants. (b) Simulated reflectance spectra of the singly asymmetric gratings with $p = 1480$ nm, $h = 230$ nm, $w_1 = w_2 = 200$ nm, and $g_1 = 400$ nm, $g_2 = 680$ nm for different ambient refractive indices (upper panel) and filling fraction I_s in the vacuum (lower panel). The inset shows the normalized electric field at GMR_{01}. (c) The blue circles are the reflectance peak positions extracted from the upper panel in (b) and plotted against n_s. The wine line is a linear fitting curve.

In the above contents, we numerically investigate the properties of BICs/quasi-BICs and GMRs hosted by suspended dielectric gratings. Experientially, these suspended structures can be fabricated by traditional lithography and etching techniques which have been demonstrated in previous works [23,48–50]. However, considering the practical applications, dielectric gratings are preferably fabricated on the surface of substrate. In this case, to achieve the BICs and GMRs, the effective refractive index of dielectric gratings must be greater than those of cladding (e.g.,

Optics EXPRESS

air) and substrate materials [51]. Hence, low-refractive-index substrate materials, such as MgF_2, CaF_2, and fused silica, are preferred. Compared with the suspended dielectric gratings, the introduction of low-refractive-index material as substrate will red shift the resonant frequencies of BICs and GMRs [52]. Besides, since the refractive index of dielectric gratings is closer to that of substrate than cladding material, more evanescent field energy exists in the substrate, which decreases the sensitivity of refractive index sensor [46,52]. Beyond that, the reduction of sensing area also degenerates the performance of sensor. Finally, the existence of substrate can allow high order propagating diffractions in the substrate so that BICs can be transformed into quasi-BICs with finite Q-factors [32].

3. Conclusion

In summary, we theoretically and numerically investigate the resonance properties of dielectric gratings with symmetric and asymmetric profiles by controlling the width of two adjacent gaps or/and Si dielectric nanobeams. The spectra and eigenmode analysis unveil that symmetric and singly asymmetric dielectric gratings both support different order GMRs and symmetry-protected BICs with symmetric and anti-symmetric magnetic field distributions under normal incidence for TM polarization. However, the change of periodicity from symmetric to singly asymmetric structure brings about some important phenomena. The fundamental BIC in symmetric structure is transformed into a leaky-mode resonance with a finite Q-factor in singly asymmetric structure due to the existence of high order diffractions. A new Fano/GMR resonance emerges at low frequency attributing to the asymmetry of gaps or Si nanobeams. Furthermore, the symmetries of gaps and Si nanobeams are broken simultaneously, a Friedric-Wintgen BIC under normal incidence is achieve due to the destructive interference of two fundamental GMRs with different localized field distributions. Benefiting from the merit of high Q-factor of fundamental GMR resonance, the asymmetric dielectric gratings are severed as a refractive index sensor. We observe that the FOM demonstrates an inverse square dependence on asymmetry parameters, but the sensitivity tends to invariability as the unchanged effective permittivity and filling fraction despite the electric field in the vacuum are greatly enhanced. A strategy of decreasing the effective permittivity is proposed to improve the sensitivity and further verified by GMR theory. Finally, we construct an asymmetric dielectric grating with a low fill factor and big period which manifests an excellent sensing performance with a near theoretical sensitivity limit of ~1506 nm/RIU and an ultrahigh FOM of ~5000.

Funding. National Natural Science Foundation of China (51902175, 51788104, 51532004); Fundamental Research Funds for the Central Universities (06500174); Beijing Municipal Science and Technology Commission (Z191100004819002); National Postdoctoral Program for Innovative Talents (BX20180153).

Disclosures. The authors declare no conflicts of interest.

Data availability. Data underlying the results presented in this paper are not publicly available at this time but may be obtained from the authors upon reasonable request.

References

1. N. K. Grady, J. E. Heyes, D. R. Chowdhury, Y. Zeng, M. T. Reiten, A. K. Azad, A. J. Taylor, D. A. R. Dalvit, and H.-T. Chen, "Terahertz metamaterials for linear polarization conversion and anomalous refraction," Science **340**(6138), 1304–1307 (2013).
2. A. Arbabi, Y. Horie, M. Bagheri, and A. Faraon, "Dielectric metasurfaces for complete control of phase and polarization with subwavelength spatial resolution and high transmission," Nat. Nanotechnol. **10**(11), 937–943 (2015).
3. M. Khorasaninejad, W. T. Chen, R. C. Devlin, J. Oh, A. Y. Zhu, and F. Capasso, "Metalenses at visible wavelengths: diffraction-limited focusing and subwavelength resolution imaging," Science **352**(6290), 1190–1194 (2016).
4. J. P. Balthasar Mueller, N. A. Rubin, R. C. Devlin, B. Groever, and F. Capasso, "Metasurface polarization optics: independent phase control of arbitrary orthogonal states of polarization," Phys. Rev. Lett. **118**(11), 113901 (2017).
5. W. T. Chen, A. Y. Zhu, V. Sanjeev, M. Khorasaninejad, Z. Shi, E. Lee, and F. Capasso, "A broadband achromatic metalens for focusing and imaging in the visible," Nat. Nanotechnol. **13**(3), 220–226 (2018).

Optics EXPRESS

6. S. Wang, P. C. Wu, V.-C. Su, Y.-C. Lai, M.-K. Chen, H. Y. Kuo, B. H. Chen, Y. H. Chen, T.-T. Huang, J.-H. Wang, R.-M. Lin, C.-H. Kuan, T. Li, Z. Wang, S. Zhu, and D. P. Tsai, "A broadband achromatic metalens in the visible," Nat. Nanotechnol. **13**(3), 227–232 (2018).
7. C. Liu, Y. Bai, J. Zhou, Q. Zhao, Y. Yang, H. Chen, and L. Qiao, "High-performance bifunctional polarization switch chiral metamaterials by inverse design method," npj Comput. Mater. **5**(1), 93 (2019).
8. P. Georgi, Q. S. Wei, B. Sain, C. Schlickriede, Y. T. Wang, L. L. Huang, and T. Zentgraf, "Optical secret sharing with cascaded metasurface holography," Sci. Adv. **7**(16), eabf9718 (2021).
9. J. Lee, M. Tymchenko, C. Argyropoulos, P.-Y. Chen, F. Lu, F. Demmerle, G. Boehm, M.-C. Amann, A. Alu, and M. A. Belkin, "Giant nonlinear response from plasmonic metasurfaces coupled to intersubband transitions," Nature **511**(7507), 65–69 (2014).
10. K. Koshelev, Y. Tang, K. Li, D.-Y. Choi, G. Li, and Y. Kivshar, "Nonlinear metasurfaces governed by bound states in the continuum," ACS Photonics **6**(7), 1639–1644 (2019).
11. N. Bernhardt, K. Koshelev, S. J. U. White, K. W. C. Meng, J. E. Fröch, S. Kim, T. T. Tran, D.-Y. Choi, Y. Kivshar, and A. S. Solntsev, "Quasi-BIC resonant cnhancement of second-harmonic generation in WS2 monolayers," Nano Lett. **20**(7), 5309–5314 (2020).
12. Y. Fan, X. He, F. Zhang, W. Cai, C. Li, Q. Fu, N. V. Sydorchuk, and S. L. Prosvirnin, "Fano-resonant hybrid metamaterial for enhanced nonlinear tunability and hysteresis behavior," Research **2021**, 1–9 (2021).
13. D. Rodrigo, O. Limaj, D. Janner, D. Etezadi, F. J. G. de Abajo, V. Pruneri, and H. Altug, "Mid-infrared plasmonic biosensing with graphene," Science **349**(6244), 165–168 (2015).
14. A. Tittl, A. Leitis, M. Liu, F. Yesilkoy, D.-Y. Choi, D. N. Neshev, Y. S. Kivshar, and H. Altug, "Imaging-based molecular barcoding with pixelated dielectric metasurfaces," Science **360**(6393), 1105–1109 (2018).
15. B. Wang, P. Yu, W. Wang, X. Zhang, H.-C. Kuo, H. Xu, and Z. M. Wang, "High-Q plasmonic resonances: fundamentals and applications," Adv. Opt. Mater. **9**(7), 2001520 (2021).
16. S. Jahani and Z. Jacob, "All-dielectric metamaterials," Nat. Nanotechnol. **11**(1), 23–36 (2016).
17. B. Luk'yanchuk, N. I. Zheludev, S. A. Maier, N. J. Halas, P. Nordlander, H. Giessen, and C. T. Chong, "The Fano resonance in plasmonic nanostructures and metamaterials," Nature Mater. **9**(9), 707–715 (2010).
18. S. S. Wang and R. Magnusson, "Theory and applications of guided-mode resonance filters," Appl. Opt. **32**(14), 2606–2613 (1993).
19. S. Fan and J. Joannopoulos, "Analysis of guided resonances in photonic crystal slabs," Phys. Rev. B **65**(23), 235112 (2002).
20. W. Zhou, D. Zhao, Y.-C. Shuai, H. Yang, S. Chuwongin, A. Chadha, J.-H. Seo, K. X. Wang, V. Liu, and Z. Ma, "Progress in 2D photonic crystal Fano resonance photonics," Prog. Quantum Electron. **38**(1), 1–74 (2014).
21. J. Jin, X. Yin, L. Ni, M. Soljačić, B. Zhen, and C. Peng, "Topologically enabled ultrahigh-Q guided resonances robust to out-of-plane scattering," Nature **574**(7779), 501–504 (2019).
22. M. Galli, S. Portalupi, M. Belotti, L. Andreani, L. O'Faolain, and T. Krauss, "Light scattering and Fano resonances in high-Q photonic crystal nanocavities," Appl. Phys. Lett. **94**(7), 071101 (2009).
23. A. Majumdar, J. Kim, J. Vuckovic, and F. Wang, "Electrical control of silicon photonic crystal cavity by graphene," Nano Lett. **13**(2), 515–518 (2013).
24. J. Li, T. P. White, L. O'Faolain, A. Gomez-Iglesias, and T. F. Krauss, "Systematic design of flat band slow light in photonic crystal waveguides," Opt. Express **16**(9), 6227–6232 (2008).
25. S. Wu, S. Buckley, A. M. Jones, J. S. Ross, N. J. Ghimire, J. Yan, D. G. Mandrus, W. Yao, F. Hatami, and J. Vučković, "Control of two-dimensional excitonic light emission via photonic crystal," 2D Mater. **1**(1), 011001 (2014).
26. C. W. Hsu, B. Zhen, J. Lee, S.-L. Chua, S. G. Johnson, J. D. Joannopoulos, and M. Soljačić, "Observation of trapped light within the radiation continuum," Nature **499**(7457), 188–191 (2013).
27. E. N. Bulgakov and A. F. Sadreev, "Bloch bound states in the radiation continuum in a periodic array of dielectric rods," Phys. Rev. A **90**(5), 053801 (2014).
28. C. W. Hsu, B. Zhen, A. D. Stone, J. D. Joannopoulos, and M. Soljačić, "Bound states in the continuum," Nat. Rev. Mater. **1**(9), 16048 (2016).
29. L. Ni, Z. Wang, C. Peng, and Z. Li, "Tunable optical bound states in the continuum beyond in-plane symmetry protection," Phys. Rev. B **94**(24), 245148 (2016).
30. L. Cong and R. Singh, "Symmetry-protected dual bound states in the continuum in metamaterials," Adv. Opt. Mater. **7**, 1900383 (2019).
31. S. Han, M. V. Rybin, P. Pitchappa, Y. K. Srivastava, Y. S. Kivshar, and R. Singh, "Guided-mode resonances in all-dielectric terahertz metasurfaces," Adv. Opt. Mater. **8**(3), 1900959 (2020).
32. Z. F. Sadrieva, I. S. Sinev, K. L. Koshelev, A. Samusev, I. V. Iorsh, O. Takayama, R. Malureanu, A. A. Bogdanov, and A. V. Lavrinenko, "Transition from optical bound states in the continuum to leaky resonances: role of substrate and roughness," ACS Photonics **4**(4), 723–727 (2017).
33. A. Kodigala, T. Lepetit, Q. Gu, B. Bahari, Y. Fainman, and B. Kanté, "Lasing action from photonic bound states in continuum," Nature **541**(7636), 196–199 (2017).
34. X. Wang, J. Duan, W. Chen, C. Zhou, T. Liu, and S. J. P. R. B. Xiao, "Controlling light absorption of graphene at critical coupling through magnetic dipole quasi-bound states in the continuum resonance," Phys. Rev. B **102**(15), 155432 (2020).

Optics EXPRESS

35. Y. Ding and R. Magnusson, "Resonant leaky-mode spectral-band engineering and device applications," Opt. Express **12**(23), 5661–5674 (2004).
36. S. Romano, M. Mangini, E. Penzo, S. Cabrini, A. C. De Luca, I. Rendina, V. Mocella, and G. L. G. Zito, "Ultrasensitive surface refractive index imaging based on quasi-bound states in the continuum," ACS Nano. **14**(11), 15417–15427 (2020).
37. S. Romano, G. Zito, S. Torino, G. Calafiore, E. Penzo, G. Coppola, S. Cabrini, I. Rendina, and V. J. P. R. Mocella, "Label-free sensing of ultralow-weight molecules with all-dielectric metasurfaces supporting bound states in the continuum," Photon. Res. **6**(7), 726–733 (2018).
38. T. Ning, X. Li, Y. Zhao, L. Yin, Y. Huo, L. Zhao, and Q. Yue, "Giant enhancement of harmonic generation in all-dielectric resonant waveguide gratings of quasi-bound states in the continuum," Opt. Express **28**(23), 34024–34034 (2020).
39. Z. Huang, M. Wang, Y. Li, J. Shang, K. Li, W. Qiu, J. Dong, H. Guan, Z. Chen, and H. Lu, "Highly efficient second harmonic generation of thin film lithium niobate nanograting near bound states in the continuum," Nanotechnology **32**(32), 325207 (2021).
40. K. Koshelev, S. Lepeshov, M. Liu, A. Bogdanov, and Y. Kivshar, "Asymmetric metasurfaces with high-Q resonances governed by bound states in the continuum," Phys. Rev. Lett. **121**(19), 193903 (2018).
41. D. N. Maksimov, V. S. Gerasimov, S. Romano, and S. P. J. O. E. Polyutov, "Refractive index sensing with optical bound states in the continuum," Opt. Express **28**(26), 38907–38916 (2020).
42. Y. Satomura, M. Matsuhara, and N. Kumagai, "Analysis of electromagnetic-wave modes in anisotropic slab waveguide," IEEE Trans. Microwave Theory Tech. **22**(2), 86–92 (1974).
43. H. Kyu-Pyung and A. C. Cangellaris, "Effective permittivities for second-order accurate FDTD equations at dielectric interfaces," IEEE Microw. Wireless Compon. Lett. **11**(4), 158–160 (2001).
44. H. Kikuta, H. Yoshida, and K. Iwata, "Ability and limitation of effective medium theory for subwavelength gratings," Opt. Rev. **2**(2), 92–99 (1995).
45. N. A. Mortensen, S. Xiao, and J. Pedersen, "Liquid-infiltrated photonic crystals: enhanced light-matter interactions for lab-on-a-chip applications," Microfluid. Nanofluid. **4**(1-2), 117–127 (2008).
46. S. Romano, G. Zito, S. Yépez, S. Cabrini, and V. Mocellaark, "Tuning the exponential sensitivity of a bound-state-in-continuum optical sensor," Opt. Express **27**(13), 18776–18786 (2019).
47. A. Sihvola, *Electromagnetic mixing formulas and applications* (Institution of Electrical Engineers, 1999).
48. M. C. Y. Huang, Y. Zhou, and C. J. Chang-Hasnain, "A surface-emitting laser incorporating a high-index-contrast subwavelength grating," Nature Photon. **1**(2), 119–122 (2007).
49. M. Davanco, M. T. Rakher, D. Schuh, A. Badolato, and K. Srinivasan, "A circular dielectric grating for vertical extraction of single quantum dot emission," Appl. Phys. Lett. **99**(4), 041102 (2011).
50. H. Kwon, T. Zheng, and A. Faraon, "Nano-electromechanical Tuning of Dual-Mode Resonant Dielectric Metasurfaces for Dynamic Amplitude and Phase Modulation," Nano Lett. **21**(7), 2817–2823 (2021).
51. S. Wang, R. Magnusson, J. S. Bagby, and M. Moharam, "Guided-mode resonances in planar dielectric-layer diffraction gratings," J. Opt. Soc. Am. A **7**(8), 1470–1474 (1990).
52. M. El Beheiry, V. Liu, S. Fan, and O. Levi, "Sensitivity enhancement in photonic crystal slab biosensors," Opt. Express **18**(22), 22702–22714 (2010).

202.119.48.81 {ts '2022-03-07 09:54:11'}